

Joint sensing of bedload flux and water depth by non-invasive seismic data inversion

Michael Dietze, GFZ German Research Centre for Geosciences, Section 4.6
Geomorphology, Potsdam, Germany (mdietze@gfz-potsdam.de),

Sophie Lagarde, Département de Géosciences, École Normale Supérieure, PSL Research
University, Paris, France (lagarde@clipper.ens.fr),

Eran Halfi, Ben-Gurion University of The Negev, Department of Geography and
Environmental Development, Unit of Environmental Engineering, Beer Sheba, Israel
(eranhalf@post.bgu.ac.il),

Jonathan B. Laronne, Ben-Gurion University of The Negev, Department of Geography and
Environmental Development, Unit of Environmental Engineering, Beer Sheba, Israel
(john@bgu.ac.il),

Jens M. Turowski, GFZ German Research Centre for Geosciences, Section 4.6
Geomorphology, Potsdam, Germany (turowski@gfz-potsdam.de)

Rivers are the fluvial conveyor belts routing sediment across the landscape. While there are proper techniques for continuous estimates of the flux of suspended solids in rivers, constraining bedload flux is much more challenging, typically involving extensive and expensive measurement infrastructure or labour-intensive manual measurements. Seismometers are potentially valuable alternatives to in-stream devices, delivering continuous high resolution data on the average behaviour of a given reach. Two models exist to predict the seismic spectra generated by river turbulence and bedload flux. However, these models require estimating a large number of parameters and the spectra usually overlap significantly, which hinders straightforward inversion. We provide a set of functions as part of the R package 'eseis' that allow generic modelling of hydraulic and bedload transport dynamics from seismic data using these models. The underlying Monte Carlo approach creates lookup tables of potential spectra, which are compared against the empirical spectra to identify the best fitting solutions. The method is validated against synthetic data sets and independently measured metrics from the Nahal Eshtemoa, Israel, a flash flood dominated ephemeral gravel bed river. Our approach reproduces the synthetic time series with average absolute deviations of 0.01--0.04 m (water depth) and 0.00--0.04 kg/sm (bedload flux). The example flash flood water depths and bedload flux are reproduced with respective average deviations of 0.10 m and 0.02 kg/sm. Our approach thus provides generic, testable and reproducible routines for a quantitative description of key metrics, hard to collect by other techniques in a continuous and representative manner.

This paper is a non-peer reviewed preprint uploaded to EarthArXiv, and submitted to the Journal Water Resources Research.

1 **Joint sensing of bedload flux and water depth by**
2 **non-invasive seismic data inversion**

3 **M. Dietze¹, S. Lagarde², E. Halfi³, J.B. Laronne³, J. M. Turowski¹**

4 ¹GFZ German Research Centre for Geosciences, Section 4.6 Geomorphology, Potsdam, Germany

5 ²Département de Géosciences, École Normale Supérieure, PSL Research University, Paris, France

6 ³Ben-Gurion University of The Negev, Department of Geography and Environmental Development, Unit
7 of Environmental Engineering, Beer Sheva, Israel

8 **Key Points:**

- 9 • We introduce a generic approach to inverting seismic records for flood water depth
10 and bedload flux
11 • Model deviations are 0.01–0.04 m (water depth) and 0.00–0.04 kg/sm (bedload)
12 throughout a range of synthetic data sets
13 • Our approach allows continuous, high resolution processing with < 0.10 m (wa-
14 ter depth) and < 0.02 kg/sm (bedload flux) deviation

Abstract

Rivers are the fluvial conveyor belts routing sediment across the landscape. While there are proper techniques for continuous estimates of the flux of suspended solids in rivers, constraining bedload flux is much more challenging, typically involving extensive and expensive measurement infrastructure or labour-intensive manual measurements. Seismometers are potentially valuable alternatives to in-stream devices, delivering continuous high resolution data on the average behaviour of a given reach. Two models exist to predict the seismic spectra generated by river turbulence and bedload flux. However, these models require estimating a large number of parameters and the spectra usually overlap significantly, which hinders straightforward inversion. We provide a set of functions as part of the R package 'eseis' that allow generic modelling of hydraulic and bedload transport dynamics from seismic data using these models. The underlying Monte Carlo approach creates lookup tables of potential spectra, which are compared against the empirical spectra to identify the best fitting solutions. The method is validated against synthetic data sets and independently measured metrics from the Nahal Eshtemoa, Israel, a flash flood dominated ephemeral gravel bed river. Our approach reproduces the synthetic time series with average absolute deviations of 0.01–0.04 m (water depth) and 0.00–0.04 kg/sm (bedload flux). The example flash flood water depths and bedload flux are reproduced with respective average deviations of 0.10 m and 0.02 kg/sm. Our approach thus provides generic, testable and reproducible routines for a quantitative description of key metrics, hard to collect by other techniques in a continuous and representative manner.

1 Introduction

Understanding the boundary conditions and non-linear dynamics of bedload transport by streams is essential for understanding process geomorphology and long term landscape evolution, but also from an engineering and hazard perspective, especially if the transport happens under episodic flood conditions. Accordingly, there has been significant effort in collecting instrumental data on important parameters determining flow characteristics and boundary conditions. Classic approaches involve either labour-intensive manual sampling (e.g., King et al., 2004; Bunte & Abt, 2005), or the permanent construction of monitoring infrastructure in the stream bed (e.g., Habersack et al., 2016). Any sensors within the stream need to be sufficiently resilient to maintain operation under the harsh conditions during flood events (Geay et al., 2017). Typical in-stream observatories include pressure gauges, temperature sensors and turbidity sensors. Bedload dynamics are monitored with time-resolving slot samplers (Cohen et al., 2010) and acoustic impact sensors, such as pipe microphones, geophones and accelerometers, or plate geophones (Mizuyama et al., 2010; Rickenmann, 2017). All acoustic bedload sensors, with the exception of hydrophones deployed in the water column (Geay et al., 2019), deliver direct and indirect data on the target parameters, provide point measurements or can at best be installed along a line crossing the channel (e.g., Hildale et al., 2014), whereas interest is often directed to the average dynamics of a given reach.

In recent years, a complementary approach has gained increasing attention: stream-side instrumentation with seismic sensors (Burtin et al., 2008; Barrière et al., 2015; Roth et al., 2016; Schmandt et al., 2017). Such sensors, typically off-the-shelf seismometers or geophones, are installed at a safe distance from the inundated channel and record the ground motion due to in-stream processes. A sensor can be deployed within less than an hour, record high resolution data continuously and autonomously for several months, and is, in principle, able to transmit the data in near real time to processing and evaluation facilities. Hence, seismic monitoring shows potential for recording bedload flux, which has recently been demonstrated under laboratory and fields conditions (Gimbert et al., 2019; Schmandt et al., 2017). However, unlike signals derived from bedload impact sensors and similar to the soundscape of rivers recorded by in-stream hydrophones (Geay et al., 2017), seismic signals derive from a multitude of sources (e.g., Roth et al.,

2017) and, therefore, the identification, extraction, and processing of signals to determine bedload flux is challenging.

Physical models have been suggested to predict the seismic frequency spectra due to bedload transport (Tsai et al., 2012) and due to hydraulic processes within a channel (Gimbert et al., 2014). Dietze (2018) has shown the principal method of using such physical models to infer water depth quasi continuously for creeks. This involved computing a lookup table of potential spectra that differ only due to changes in river depth and identification of the best reference data fits to the time series of empirical spectra. Here, we expand this approach to bedload flux, based on the notion that the spectra generated by turbulence and bedload transport should be sufficiently distinct (cf. Gimbert et al., 2014; Dietze et al., 2019). In our approach, fits of the empirical data with pre-calculated reference spectra are optimised based on random combinations of the target parameters. Applying the approach to a case study at the Nahal Eshtemoa, Israel, we show how seismic stations can be used to continuously estimate key hydraulic and bedload transport parameters. We explore the validity of the approach based on synthetic data and by comparing the model output against independent measurements of target parameters. We show the value of seismic stations to gather insight on the anatomy of bedload transporting floods, and discuss potentials and limitations of the technique.

2 Materials and methods

2.1 Study site and instrumentation

The Nahal (river) Eshtemoa is an ephemeral, flash flood dominated gravel bed river in the semi-arid northern Negev Desert, Israel, draining the southern Hebron mountains in a catchment of about 112 km². Close to the town of As-Samu, the stream crosses a gently undulating landscape in an alluvial valley. A straight, 5 m wide reach with 1 m high banks is instrumented by a comprehensive in-stream observatory (Laronne et al., 1992), including Reid-type slot samplers, plate geophones, a pipe microphone, water quality sensors and sampler, as well as pressure transducers for the determination of water depth and water surface slope. Since 2016, a Nanometrics TC120s broadband seismometer has been installed in the right bank (Fig. 1 a, b). It is sampled by a Nanometrics Centaur data logger at a recording frequency of 200 Hz and a gain of 2.

2.2 Computational environment

The R package 'eseis' (Dietze, 2018) is a free and open source toolbox for handling the work flow of generic environmental seismology. With the latest developer version (0.5.0) it contains models to predict the seismic spectrum due to turbulent channel flow (Gimbert et al., 2014), and impacting bedload particles (Tsai et al., 2012). Both models can be explored in an interactive graphical user interface (GUI) (Fig. 2). Three additional functions, denoted by the prefix *fmi*, are devoted to the approach of fluvial model inversion presented in this study. Data preparation, processing, analysis and visualisation steps were performed with R v. 3.5.3 (RCoreTeam, 2015). The R functions, data sets and utilised scripts are available as commented markdown files in the supplementary materials to reproduce the presented results.

2.3 Data processing

Flood water depth and bedload flux time series were recorded at minute resolution. The bedload flux time series starts when at least 4 kg of sediment have been collected in the slot samplers during an event, which represents the sensitivity threshold of the sensors. We used the median of the values measured by the three bedload samplers to generate a representative bedload flux per unit stream width. The recorded seismic files were converted to hourly SAC files and organised in the consistent structure as used by

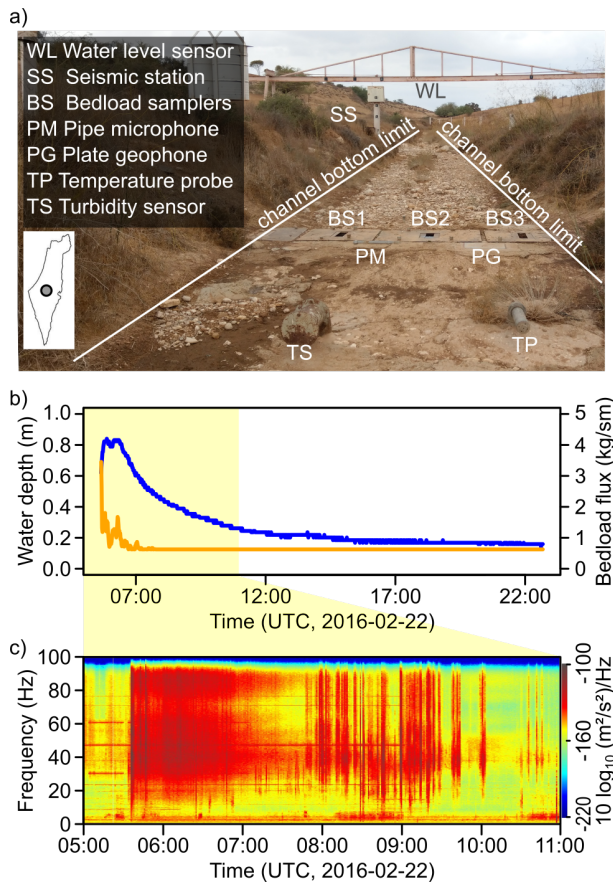


Figure 1. Study site, instrumentation and example flood event. a) View upstream of the flash flood prone Nahal Eshtemoa, Israel. At this location, an in-stream observatory records many essential hydraulic, sediment transport and chemical parameters. A broadband seismometer is installed at the true right bank. b) Hydrograph and bedload flux data from an example flood event; yellow background denotes period of interest. c) Spectrogram of the example flood as recorded by the seismometer.

115 the functions of the 'eseis' package. For the relevant part of the flood (05:40 to 11:00 UTC,
 116 cf. Fig. 1 b) we calculated a spectrogram from the vertical component of the seismic time
 117 series using the method of (Welch, 1967) with 10 s long, non-overlapping windows, av-
 118 eraging 5 s long and 80 % overlapping sub windows.

119 2.4 Model approach

120 Our approach assumes that the recorded seismic spectrum is dominated by chan-
 121 nel activity, i.e., a combination of turbulent flow and sedimentary particles impacting
 122 the channel floor during bedload transport, whereas other sources such as the effects of
 123 wind and rain, or anthropogenic activity are of subordinate importance. Under these con-
 124 ditions, we can exploit the combination of the seismic models of Tsai et al. (2012) and
 125 Gimbert et al. (2014). Specifically, we used a Monte Carlo approach to randomly vary
 126 the two parameters of interest, water depth and bedload flux, to generate 5000 differ-
 127 ent potential seismic conditions that serve as a look up table. In addition, to account
 128 for flow without bedload transport, we calculated another 1000 realisations where bed-
 129 load flux was set to zero and only water depth was varied. In the Nahal Eshtemoa case,
 130 we allowed water depth (h_w) to range from 0.01 m (minimum value required to allow
 131 model evaluation) to 1.20 m (120 % of bankfull depth). Bedload flux q_s was varied be-
 132 tween 0 kg/sm and 15 kg/sm (200 % of the range reported for other floods, (cf. Cohen
 133 et al., 2010)). The selected boundaries are arbitrary and can be extended, if needed –
 134 for example, when the model output yields values that clearly undershoot the expected
 135 empirical data. For each parameter combination, we calculated a seismic reference, and
 136 calculated root mean square errors with the corresponding observed spectrum. For each
 137 time step, we then selected the values for water depth and bedload flux corresponding
 138 to the artificial spectrum with the smallest root mean square error. To account for short
 139 term variability of the seismic record, the model results were smoothed with a running
 140 average (R package caTools v. 1.17.1.2, (Tuszynski, 2014)) using a window size of 18 sam-
 141 ples, i.e. 180 s.

142 2.5 Estimation of unknown model parameters

143 Both the turbulence (Gimbert et al., 2014) and the bedload (Tsai et al., 2012) model
 144 require constraints on a set of 17 parameters (Table 1). Some of these parameters can
 145 be determined from field measurements, namely the median grain size D_{50} (d_s), logarith-
 146 mic grain size standard deviation (s_s), channel width (w_w), channel bed gradient (a_w),
 147 and the distance between the centre line of the river and the seismic station (r_0). Other
 148 parameters can be estimated at reasonable accuracy based on prior measurements, such
 149 as the specific density of the fluid (r_w) and of the bedload material (r_s). And yet oth-
 150 ers are simply set according to computational needs and convention, such as the refer-
 151 ence frequency (f_0), frequency range (f) and resolution (res) for which the model yields
 152 results. Several parameters describe the seismic ground characteristics due to the site
 153 properties. This set of parameters (material quality factor q_0 and its increase with fre-
 154 quency e_0 , Rayleigh wave phase velocity at the reference frequency v_0 and its variation
 155 coefficient p_0 , and the Greens function displacement amplitude coefficients n_0) can be
 156 constrained by performing an active seismic survey. However, when that is not possible,
 157 they must be estimated.

158 In a first step we make use of the interactive GUI provided with the R package 'eseis'
 159 (Fig. 2). This application allows changing all relevant model parameters and instan-
 160 taneously plots updated model outputs, together with an optionally provided empirical
 161 spectrum. We used this tool to explore the meaningful parameter space, which is able
 162 to create model spectra that match the overall shape and amplitude of a series of em-
 163 pirical spectra. We focused on empirical spectra at the beginning of the flood event, where
 164 sharp rises of broadband seismic signals (Tsai et al., 2012; Schmandt et al., 2017) indi-
 165 cate pulses of bedload movement close the seismic sensor, and later stages of the flood,

Seismic spectra model visualisation

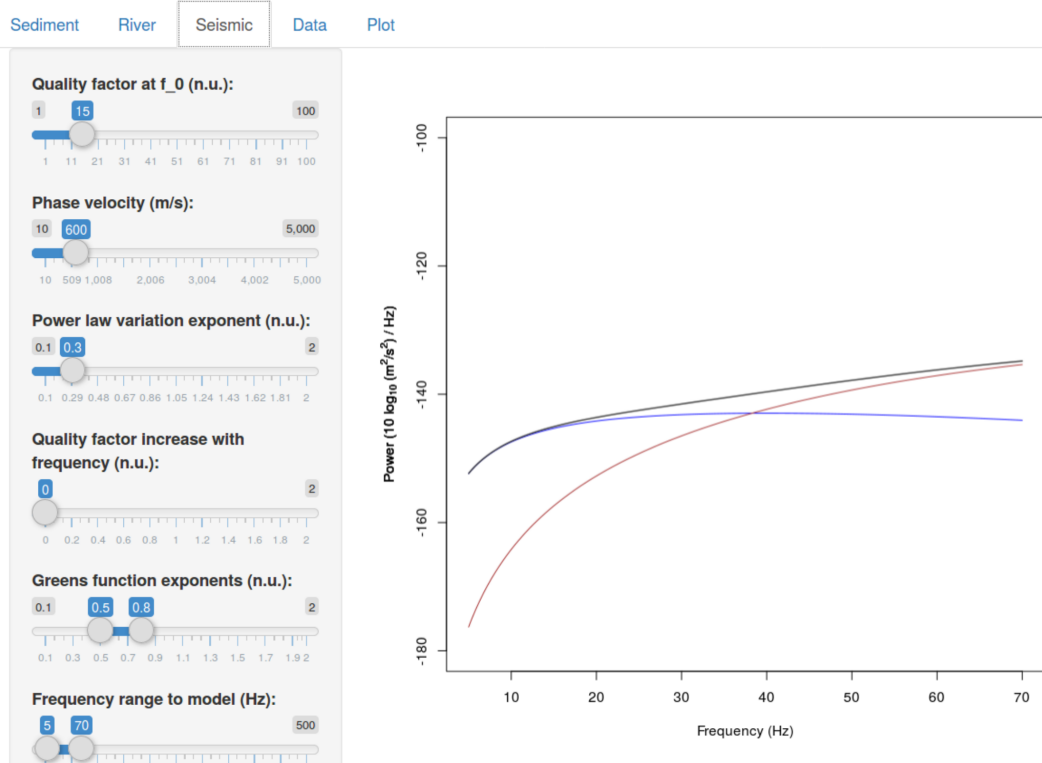


Figure 2. Interactive GUI of the seismic models, available through the R package 'eseis'. The application can be used to explore the effect of model parameters. It allows changing all relevant model parameters and generates instantaneous updates of the results. The blue line depicts the result of the water turbulence model, the red line shows the bedload model output and the black line illustrates the combined model spectrum.

Table 1. Model parameter values and their associated uncertainties. Target parameter ranges for identifying the most plausible ones are given in parentheses. * (Cohen et al., 2010)

Parameter (unit)	Symbol	Nahal Eshtemoa
D_{50} bedload grain diameter (m)	d_s	0.01*
Grain diameter standard deviation (log m)	s_s	1.35*
Bedload flux (kg/sm)	q_s	0–20
Sediment density (kg/m ³)	r_s	2650
Fluid density (kg/m ³)	r_w	1040
Water depth (m)	h_w	0.01–1.20
Average channel width (m)	w_w	5
Channel slope (radians)	a_w	0.0075*
Distance river to station (m)	r_0	5.5
Reference frequency (Hz)	f_0	1
Model frequency range (Hz)	f	10–70
Material quality factor at f_0 (s.d.)	q_0	16.77 (15–20)
Rayleigh wave phase velocity at f_0	v_0	859 (800–900)
Variation coefficient for v_0	p_0	0.62 (0.4–0.7)
Q increase with frequency (s.d.)	e_0	0.07 (0.01–0.25)
Greens function displacement amplitude coefficients (s.d.)	n_0	0.5, 0.8

166 when the bedload signal is no longer visible in the seismic spectrogram and most of the
167 seismic signal is presumably generated by turbulence. We adjusted the parameters q_0 ,
168 v_0 , p_0 , e_0 and n_0 to roughly match the shape of the resulting fluvial, bedload and joint
169 spectra to the empirical example spectra mentioned above. Thereafter, we changed the
170 parameters water depth and bedload flux to adjust the seismic power of the model spec-
171 tra until they visually matched the empirical spectra. The quality of the match was sub-
172 sequently quantified and optimised by minimising the root mean square error. From this
173 set of combinations optimized to first order we started changing the seismic parameters
174 towards lower and higher values, respectively, until the match of empirical and model
175 spectra obviously diverged. We defined these parameter ranges as the limits for the sub-
176 sequent step of parameter range optimisation. In a second step we performed the inver-
177 sion of the example flood data set in an extended Monte Carlo experiment. Since the
178 lower and upper Greens function parameters n_0 did not have significant impact on the
179 model spectra shape when changing them between 0.4 and 0.8 and 0.5 and 0.9, respec-
180 tively, we set them arbitrarily to 0.5 and 0.8. We created 10^5 random parameter com-
181 binations of the most sensitive parameters (q_0 , v_0 , p_0 , e_0) and the target parameters (h_w
182 and q_s), exploring the range of the former set of parameters to identify the most likely
183 values throughout the event (i.e., the medians of the distributions).

184 2.6 Model validation

185 In order to infer the ability of the model approach to estimate water depth and bed-
186 load flux, we created several synthetic data sets, inverted them and compared the result-
187 ing model time series of the target parameters to the input data (Fig. 3). Synthetic data
188 set 1 imposes a constant water depth of 0.5 m. The bedload is injected after 2 h of the
189 modelled time period (6 h), resulting in an instantaneous rise to 5 kg/sm, which is held
190 constant for another 2 h until it is reduced linearly to zero for the rest of the time. This
191 data set is mainly used to test the sensitivity of the model to fluctuations in a param-
192 eter when the other is changed. Synthetic data set 2 assumes synchronously rising and
193 falling water depth and bedload flux, both of which are modelled as lognormal distri-
194 bution curves. This scenario reflects a river where water depth and bedload flux do not

195 show a hysteresis effect and where the seismic signal overlap is constant through time.
 196 Synthetic data set 3 features a lognormal bedload time series that rises steeper and nar-
 197 rower than the lognormal water depth time series, thus generating a bedload wave trav-
 198 elling in front of the flood wave. This scenario inherits a clockwise hysteresis pattern.
 199 Synthetic data set 4 uses the empirically measured water depth and bedload flux val-
 200 ues to generate a seismic spectrogram. It is used to explore how precisely the target vari-
 201 ables can be estimated by the model approach under ideal conditions: all signals of the
 202 spectrogram are only caused by flowing water and bedload flux.

203 Model quality is assessed by the absolute difference between synthetic and best fit
 204 modelled reference spectra. This error can be studied both in time and frequency space.
 205 Another measure of model quality is the error (residual) between water depth or bed-
 206 load flux and the respective model estimates.

207 **3 Results**

208 **3.1 Characteristics of the flood**

209 The flood hydrograph shows a rapid rise of water depth although the actual on-
 210 set of the event is not shown here because we define the event by the onset of the bed-
 211 load sampler records, i.e., at 05.40 UTC. After the flood’s double peak occurred (0.84
 212 and 0.83 m), water depth dropped logarithmically for at least 13 h (Fig. 1 b). The three
 213 bedload samplers monitored a maximum average value of 4.29 kg/sm. The highest bed-
 214 load fluxes were recorded within the first two minutes. Thereafter values declined pro-
 215 gressively to almost zero around 05:55 UTC, when two further, smaller bedload waves
 216 (peak flux 1.08 kg/sm) emerged for 30 min. Bedload transport ceased at 07:10 UTC. With
 217 the onset of the flood, the seismic spectrogram shows a broadband (10–90 Hz) increase
 218 in seismic power up to -100 dB, which progressively grades into background for about
 219 one hour. At about 07.50 UTC, a period of broadband spike appearance occurs that lasts
 220 for at least 2.5 h.

221 **3.2 Model validation with synthetic flood time series**

222 The ability of the model to reconstruct the synthetic time series of target param-
 223 eters (which were used to generate noise-free spectrograms that were inverted) provides
 224 the accuracy baseline for the actual inversion of the empirical data set. Synthetic data
 225 set 1 (Fig. 3 a) yielded absolute differences between best fit model and input spectro-
 226 gram of less than 0.5 dB and target parameter errors of 0.02 ± 0.04 m (water depth) and
 227 -0.03 ± 0.06 kg/sm (bedload flux). The modelled time series resemble the onset of changes
 228 and are only slightly affected by changes in the corresponding parameter. Synthetic data
 229 set 2 (Fig. 3 b) has only minor spectral differences (less than 0.26 dB) and model errors
 230 (0.02 ± 0.04 m and -0.06 ± 0.13 kg/sm, respectively). The concurrent changes in water depth
 231 and bedload flux are captured well. However, during the second half of the synthetic event
 232 the model produced increasingly larger deviations. Synthetic data set 3 (Fig. 3 c) has
 233 the largest spectral differences (up to 1.75 dB), but yielded the smallest target param-
 234 eter errors (-0.01 ± 0.03 m and -0.001 ± 0.03 kg/sm, respectively). These errors mainly ap-
 235 pear towards the end of the synthetic data set, when the continuously declining water
 236 depth curve is represented by step-wise model results. The synthetic data set produced
 237 by the real world time series of water depth and bedload flux (Fig. 1 b) produced spec-
 238 tral differences of up to 0.47 dB and target parameter errors for water depth and bed-
 239 load flux of -0.04 ± 0.03 m and -0.001 ± 0.02 kg/sm, respectively. The water depth is thus
 240 overestimated, especially when bedload transport ceases.

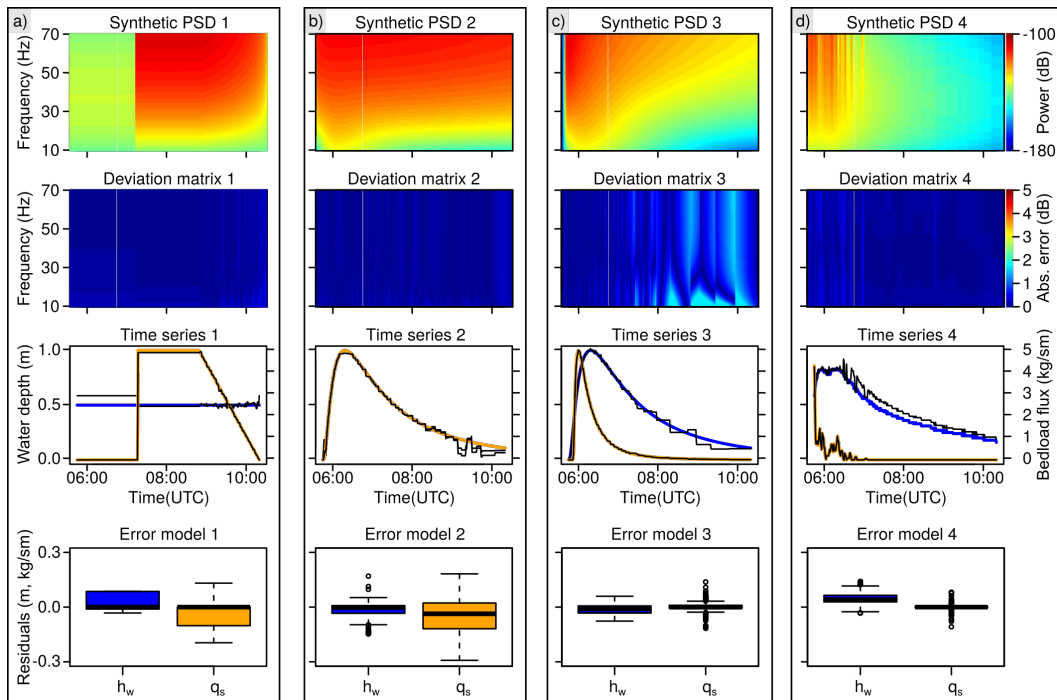


Figure 3. Model validation summary. Four synthetic data sets were tested, and are organised by columns a-d). Each panel shows the resulting synthetic spectrogram, the fit deviation matrix depicting the root mean square error between empiric spectra and best fit reference spectra, the input (blue line shows water depth, orange line bedload flux) and modelled time series (black lines), and the distribution of model errors (residuals) in target parameter units.

3.3 Model parameter estimation

Explorative model parameter adjustments (Fig. 2) revealed that the shape of the fluvial and bedload model spectra can vary significantly. In turn, the parameter range that lets the models and their summed effect converge in shape to those of the empirical spectra during the peak water depth and the falling limb of the flood is small. Thus, we defined the limits within which q_0 was allowed to vary to 15–20, for v_0 to 800–900 m/s, for p_0 to 0.4–0.7 and for e_0 to 0.01–0.25 (cf. Tab. 1). As expected, changes in the input parameters water depth and bedload flux result in amplitude shifts with no visible effects on the shape of the spectrum (Fig. 4 a). In contrast, higher ground quality factors (Fig. 4 b) lead to systematic counter-clockwise rotation effects of the spectra until the spectral power rises monotonously with increasing frequency, which is not visible in the empirical data (Fig. 1 c). A similar effect occurs for the Rayleigh wave phase velocity v_0 (Fig. 4 c), although increasing velocity values do not cause higher spectral power as is the case for the quality factor. The wave velocity variation coefficient p_0 (Fig. 4 d) mainly affects the amplitude of the bedload spectrum and the convexity of the turbulence spectrum. The parameter describing quality factor increase with frequency e_0 (Fig. 4 e) shows similar effects with value changes like the quality factor. However, this parameter is not included in the turbulence model and has therefore no effect on the latter.

Running the Monte Carlo approach with the range of seismic parameters as defined in Tab. 1 yielded convergent results with median values and quartiles of the distributions well within the defined parameter range (Fig. 4 f). The effect of the parameters is independent of each other. Thus, the best fitting combination of parameters for each of the 10 s long empirical spectra can in principle be anywhere within that imposed range. Since this is not the case the parameter distribution is assumed to be unimodal and adequately represented by the median as a most likely value. Therefore, we chose the medians ($q_0 = 16.77$, $v_0 = 859$, $p_0 = 0.62$, $e_0 = 0.07$) for the subsequent Monte Carlo run to estimate the actual target parameters.

3.4 Model results for the empirical data set

The seismic data of the example flood event (Fig. 1 c) shows contribution of the expected frequency bands between 5 and 70 Hz (Tsai et al., 2012; Gimbert et al., 2014; Schmandt et al., 2017). However, above 70 Hz there is increased seismic energy. That pattern appears to be a horizontally flipped version of the < 70 Hz signals and cannot be physically explained. Therefore, and to avoid introducing a systematic bias, we truncated the spectrogram to the frequency range 10–70 Hz, an interval to which the seismic models are most sensitive. Furthermore, to reduce scatter in the frequency domain and to improve computational speed (the frequency vector of the raw spectrogram had 1000 values), we spline-interpolated the frequency vectors of the spectrogram to 100 values between 5 and 70 Hz, corresponding to the modelled spectra (cf. supplementary materials I).

The best fit spectra deviations (Fig. 5 b) range between 0 and 15 dB. The highest deviations appear at the continuous narrow band signals (23, 47 Hz) as well as during the period with numerous short term, broadband signals (7:50–10:10 UTC). Smaller deviations, up to 10 dB occur during the early stage of the flood (5:40–7:50 UTC). They affect the upper and lower frequencies of the modelled spectra as well as the central bands (30–45 Hz).

The modelled water depth (Fig. 5 c) is in general agreement with the independent water depth measurements, although the falling limb of the flood is underestimated by 0.10 m on average (i.e., median of the absolute deviations). During 7:50 and 10:10 UTC (grey polygon in Fig. 1), when the spectrogram (Fig. 5 a) exhibits several broadband spikes, the model shows significant overestimation effects. Overall, the seismic results are more variable than the one minute resolution control data (180 s running standard deviations

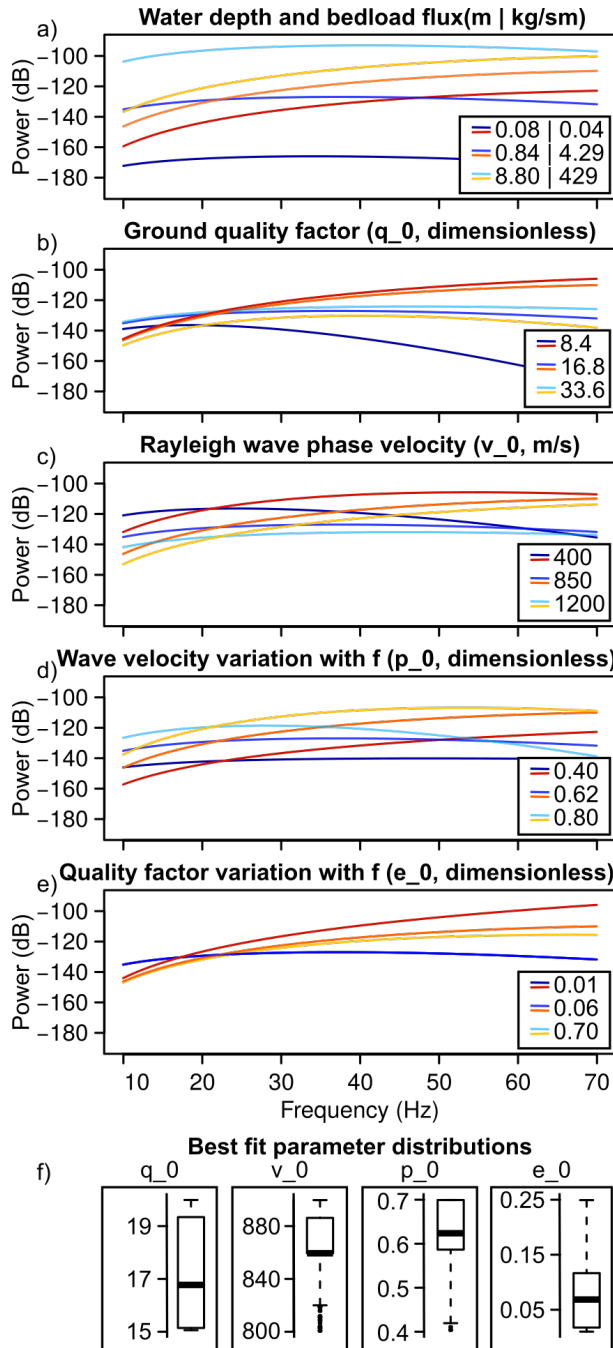


Figure 4. Visual and Monte Carlo based exploration of model sensitivity. a) Effect of the variation of water depth and bedload flux on model spectra. b) Effect of the variation of ground material quality factor. c) Effect of the variation of Rayleigh wave phase velocity. d) Effect of the variation of wave velocity variation coefficient. e) Effect of the variation of quality factor variation with frequency. Red to orange lines depict output of the bedload model, blue lines show turbulence model results. In both cases the numbers in the legend refer to the values of the changed model parameters. f) Boxplots showing the range of seismic model parameters that yielded the best fit results of the model inversion. The median values were used for the final estimation of water depth and bedload flux (cf. Table 1).

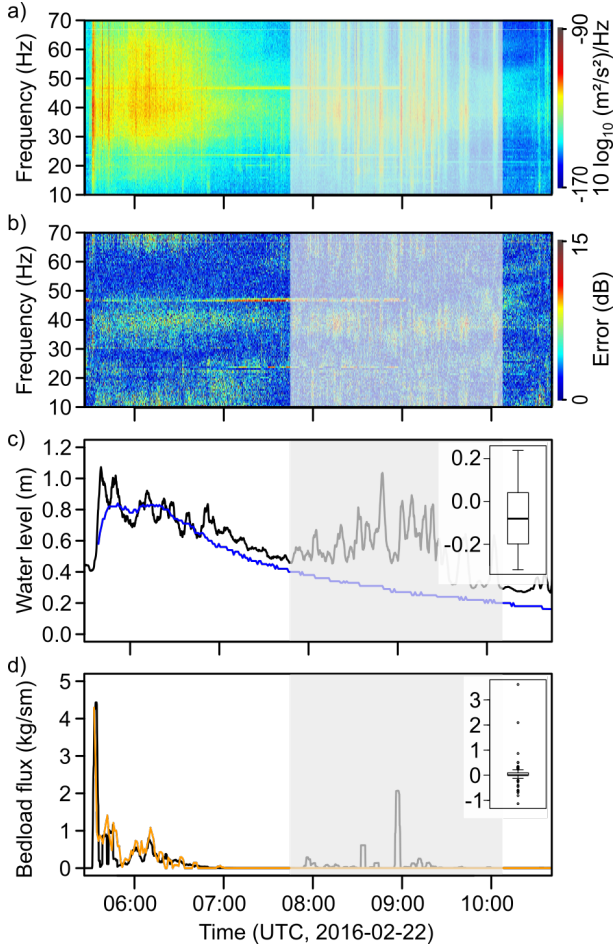


Figure 5. Results of the empirical data set inversion. a) Truncated (10–70 Hz) and aggregated (100 frequency values) spectrogram. b) Deviations of model fits resolved by time and frequency. c) Modelled (black line) and empirically measured water depth (blue line). d) Modelled (black line) and independently measured (orange line) bedload flux values. Note that in c) and d) the model results are smoothed by a 180 s running average filter. Grey polygons indicate a period with signal contamination. Boxplots give residuals of model versus empirical data.

292 of 0.041 versus 0.029 m). Results of seismic bedload flux are also in the same range as
 293 the slot sampler data (0.02 kg/sm average deviation), and most of the short excursions
 294 of increasing and decreasing bedload flux values in the slot sampler time series are co-
 295 incident with the seismic model results, both in terms of timing and amplitude.

296 4 Discussion

297 4.1 Model quality

298 The synthetic data sets (Fig. 3) allow insight on three different dimensions. First,
 299 they show the general applicability and validity of the Monte Carlo-based inversion ap-
 300 proach. Second, they provide the baseline of accuracy, i.e., the minimum deviations to
 301 expect when modelling an empirical data set. Third, the scenarios allow insight as to how
 302 different combinations of flood and bedload flux evolutions appear in seismic spectro-
 303 grams.

304 In all cases, the input time series were depicted by the model, with deviations of
 305 less than 0.04 m for water depth and 0.04 kg/sm for bedload flux. Thus, for inversions
 306 of empirical data sets one should anticipate at least these ranges of model deviations.
 307 Under the ideal conditions of synthetic data sets generated without any noise or contri-
 308 bution of additional seismic sources, the deviations of the best fit reference spectra from
 309 the synthetic spectra time series (deviation matrices in Fig. 3) are negligible. An excep-
 310 tion is test data set 3 (Fig. 3 c), which shows misfits of up to 2 dB coincident with the
 311 step-like evolution of the modelled water depth during times of virtually zero bedload
 312 flux. This step-like behaviour disappears when more than the 1000 Monte Carlo cycles
 313 are used to generate the reference spectra (not shown). Thus, it is important to provide
 314 a sufficiently large number of potential parameter combinations for the reference spec-
 315 tra, especially when high fit qualities for the falling water depth limb are of interest. A
 316 similar effect is visible in the fourth synthetic data set (Fig. 3 d) and, to a lesser degree
 317 also in data set 2, where the falling water depth curve is systematically overestimated
 318 as soon as bedload flux fades.

319 The imposed time series of synthetic data set 1, constant water depth and a step-
 320 like onset of bedload movement, are far from what one would expect in natural systems.
 321 However, this scenario shows that model deviation is systematically higher for times when
 322 only one of the two expected seismic sources is active (i.e., water depth is overestimated
 323 when no bedload is transported). In the case of synchronous evolution of flood stage and
 324 bedload flux (data set 2) the model results maintain this synchronicity. This is encour-
 325 aging because when a seismically derived data set exhibits such a pattern it is difficult
 326 to judge merely from the properties of the spectra, whether there indeed are two seis-
 327 mic sources present. In the case of a bedload wave travelling in front of a flood (Fig. 3 c),
 328 i.e., a clock-wise hysteresis pattern in the h_w-q_s relationship, the combined effect of tur-
 329 bulence and bedload movement result in a spectrogram with a trend of rising dominant
 330 frequency with time. Such patterns were observed in natural settings, such as a flash flood
 331 observatory in New Mexico (Dietze et al., 2019) but could not be attributed to a likely
 332 cause. Here, we can provide this cause, which is simply the combination of two seismic
 333 sources with different time evolution paths. The trend towards higher frequencies remains
 334 visible without any hysteresis effect, albeit weaker (e.g., Fig. 3 b). Since even water depths
 335 up to 0.5 m only contribute as much as -135 dB to the total seismic signal (Fig. 3 a), it
 336 appears that most of the seismic energy is contributed by the bedload part at this dis-
 337 tance of channel to sensor.

338 4.2 Evolution of the flood event

339 The example event shows the typical features of flash floods in the Nahal Eshte-
 340 moa (Halfi et al., 2018): a suddenly rising water depth that remains unstable due to the
 341 high turbulence and a bedload bore at the front of the flood, occasionally followed by
 342 further bedload bores. The passing of these bores are recorded in the example flood by
 343 both the slot samplers and the seismic sensor (Fig. 5 d and a), the latter showing this
 344 as broadband spikes of seismic energy after the onset of the flood. With the end of the
 345 bedload transport period the spectrogram only shows noticeable seismic energy between
 346 20 and 50 Hz that gradually decreases in amplitude with time.

347 This trend is interrupted between 07:50 and 10:10 UTC (grey shaded area in (Fig. 5)
 348 by recurring broadband seismic pulses. We interpret these pulses as the effects of per-
 349 sons working at the observatory for data collection and station maintenance reasons. These
 350 activities included walking and operating at close proximity to the seismic sensor and
 351 a car idling at the bank. A further set of seismic signals, the temporally constant, nar-
 352 rowband horizontal lines in the spectrogram (Fig. 1 c) around 22 and 44, 30 and 60 Hz,
 353 is interpreted as the signature of measurement devices operating at the observatory. When
 354 excluding this period of signal contamination, the temporal variation of the seismic signal-
 355 derived bedload flux shows three important components of the average-channel bedload

flux: (i) A first very large wave in bedload flux up to 5 kg/sm, which drastically recedes within minutes of the arrival of the flood bore, (ii) a second multiple-rise peaking at about 1 kg/sm, and (iii) and a third, smaller rise (0.5 kg/sm) with a long, 1 h recession. Given the 120 s averaging required with respect to the sensitivity of the slot sampler bedload monitoring equipment, it is remarkable that a single sensor deployed on the bank of a river can determine the main and relative features of bedload flux.

4.3 Benefits, limitations and outlook

In comparison to classic approaches to constraining hydraulic and sediment transport parameters in fluvial systems the seismic method introduced here shows several advantages. The sensors can be deployed easily and quickly, at a safe distance from the hazardous conditions of flood-prone streams. Modern seismic stations can record ground motion data at high frequency, under harsh conditions and even transmit the data in near real time to analysis facilities where they can be automatically analysed. In the case shown here, and once the data set of reference spectra is pre-calculated, inverting an empirical spectrum requires less than one second computation time on a single CPU. Thus, efficient and near real time information about floods and the potentially hazardous bedload they transport can be provided also for remote locations in a continuous manner.

While classic approaches, such as slot samplers are only able to measure the bedload flux at discrete cross-sectional intervals (the slot aperture in the Nahal Eshtemoa observatory is 11 cm and the devices are spaced about 1 m) and a representative estimate of bedload flux must be based on averaging data of several samplers, the seismic approach implicitly provides an estimate for a longer reach. The size of that reach may be approximated by changing the parameter distance to river r_0 in the interactive GUI (Fig. 2). However, a more robust field experiment with actively moved pebbles in the channel would be more appropriate (cf. Schmandt et al., 2017).

None of the available bedload formulae can replicate such natural fluvial sediment wave phenomena as presented here (e.g., Gomez et al., 1989; Cudden & Hoey, 2003), even though theoreticians, notably Einstein (1950) and experimentalists (e.g., Iseya & Ikeda, n.d.; Lisle et al., 2001; Aberle et al., 2012; Ghilardi et al., 2014; Dhont & Ancey, 2018) have long been aware of their presence. Indeed, based on a century of geomorphological research, it is known that fluvial systems are complex (Schumm, 1991, 2005); they do not transport bedload at certain time scales as simply as does an "efficient" machine (Bagnold, 1966), nor merely determined by average reach shear stress (Parker, 1990). Instead, the fluvial system responds in complex manners, as in this case one sensor and the respective technique demonstrate. With the seismic approach we are able to provide robust and high resolution field data which are crucial to determine river activity, river stability, river change and the transport of bedload to various ecologically sensitive reaches, to reservoirs and to the oceans.

However, in comparison to classic methods, the seismic approach also has drawbacks. First, the recorded signals represent measurements of ground velocity due to a multitude of sources, which are inverted for the parameters of interest using a combination of physical models. These models are formulated under a series of assumptions (cf. Tsai et al., 2012; Gimbert et al., 2014) and require information about a large number of parameters. Although the model output is in appropriate physical units (m and kg/sm) that does not require development of a further transfer function, they are not direct measurements of the parameters of interest. This point also needs to be considered in the light that the seismic approach does not necessarily reflect the same process as, for example the Reid type sampler, which records all particles that fall through the 11 cm wide slot while omitting all particle that pass between two such slots. The seismic record is an amalgam of the impacts of all bedload particles in a given reach and

406 therefore provides a spatially integrated result, which may differ from spatially discrete
 407 direct measurements due to cross sectional non-uniform bedload fluxes.

408 The selection of seismic model parameters is crucial for the inversion results. Thus,
 409 at best one performs an active seismic survey to independently constrain these param-
 410 eters. Since this was not possible in this study, we introduced a step-wise approach as
 411 an alternative: i) visual exploration of parameter effects on model output with respect
 412 to empirical seismic observations under partly known flood conditions (Fig. 2), ii) long
 413 Monte Carlo chains to identify the parameter combination that best explains the em-
 414 pirical data set (Fig. 4 f), before iii) actually inverting the data with the most plausi-
 415 ble set of parameters (Fig. 5) along with relevant metrics for model errors.

416 Seismic sensors are not only subject to the seismic sources of interest but also record
 417 a range of further processes, as the period of maintenance activities shows. Atmospheric
 418 processes such as wind and rain (Dietze et al., 2017; Roth et al., 2017) generate seismic
 419 signals in a similar frequency range. Burtin et al. (2008) and Cook et al. (2018) showed
 420 that the seismic footprint of rivers and the bedload they transport can be detected over
 421 tens of kilometres. Thus, trunk streams close-by may also add their seismic signature
 422 to the signals recorded at the stream of interest. Therefore, the deployment site for a
 423 seismic station intended to record water depth and bedload flux must be chosen with care.
 424 They should be out of the range of unwanted seismic sources such as roads and railroads,
 425 industrial buildings with running machines, should be shielded from the signals of wind
 426 and rain (at best by burying the sensor several decimetres to metres in the ground) and
 427 be installed several kilometres from other neighbouring streams. If the latter is not pos-
 428 sible, the Monte Carlo based inversion must include the other stream as an additional
 429 source of water turbulence and bedload transport.

430 The approach is vulnerable to transgressive or sudden changes in one or more of
 431 the seismic model parameters, for example if soil moisture changes drastically or frozen
 432 ground thaws during the summer period, both of which cause changes in the seismic wave
 433 velocity and quality factor (James et al., accepted). Likewise, reorganisation of the chan-
 434 nel bed by mobilisation, re-deposition, and injection of material, e.g. from bank failures,
 435 can change some of the parameters assumed to be stable. Finally, floods beyond bank
 436 full depth will result in a sudden and significant change in parameters such as width and
 437 depth. Mathematically, the models might be calculated for the different cross sections
 438 of the suprabank new river, but this would require setting up more extensive synthetic
 439 data sets and exploring the quality of the results of combined model spectra from mul-
 440 tiple independent river cross sections.

441 Future applications of the seismic approach introduced here could be near real time
 442 warning systems or continuous observation devices for streams otherwise hard to instru-
 443 ment, for example due to conservation requirements or steep topography. In principle,
 444 it is also possible to survey large, navigable rivers with high bedload fluxes during floods,
 445 as long as the position of the sensor(s) is chosen carefully to minimise the overlap of spec-
 446 tral components and recording of other seismic sources. A continuous record of bedload
 447 transport in combination with high resolution time series of suspended sediment load
 448 opens the perspective for the holistic view on catchment-wide sediment dynamics. Fi-
 449 nally, installation of a series of sensors along a stream over a greater distance allows for
 450 tracking and detailed insight into flood waves, as recently highlighted for a lake outburst
 451 flood in Nepal (Cook et al., 2018). The generic layout of the inversion approach, as il-
 452 lustrated during the seismic parameter range estimation, can in principle be used to in-
 453 vert for parameters other than water depth and bedload transport, as well. Given that
 454 all model parameters are well constrained, one can explore reorganisation of the bed by
 455 comparing model fits with respect to grain-size distribution parameters (s_d and s_s) from
 456 data before and after a flood event.

5 Conclusions

The seismic method is a valid approach to quantifying key hydraulic and bedload transport parameters, not merely as proxy data in its own data dimension and unit space (i.e., dB), but as estimates of the target parameters in the respective units: water depth in metres and bedload flux in m^3/s or kg/sm . However, this is only possible if i) one or more stations are placed at appropriate distances from the river as seismic source, ii) the empirical data are free of (or cleaned from, (e.g., Bottelin et al., 2013)) unwanted signal components, and iii) the relevant model parameters are sufficiently well constrained, either by independent measurements or at least by optimising free parameters with respect to the target parameters during a control period. The approach yields a quasi-continuous output with relative deviations of 0.10 m (water depth) and 0.02 kg/sm (bedload flux), respectively.

The comparably uncomplicated and quick installation, potential of almost real time data transmission and quick processing render the seismic approach a complementary source of data otherwise difficult to obtain. This opens up perspectives such as exploring the boundary conditions that control the onset of motion in episodically active river systems, investigating the coupling of processes that shape different landscape elements such as rock walls, debris flows, bank failures, and migrating rivers, and deliver high resolution field data to long-standing concepts of fluvial geomorphology.

The model code has been implemented using a user-driven, free and open software environment. Sensors and data loggers are becoming more and more affordable. The density of existing seismic networks along with the availability of their measurement data increases progressively. These three tendencies provide the base for other scientists to engage with the method, develop their own measurement systems or make use of the large amount of existing data to pursue their research hypotheses.

Acknowledgments

Seismic and stream observatory data, as well as analysis scripts and R functions are available in the supplementary materials. This study was funded by the Israel Science Foundation grant 832/14 to JBL. MD is funded through the H2020 Marie Curie action ITN SUBITOP (Grant number 674899). All field work was supported by GFZ internal funds.

References

- Aberle, J., Coleman, S., & Nikora, V. (2012). Bed load transport by bed form migration. *Acta Geophysica*, *60*, 1720–1743.
- Bagnold, R. (1966). An approach to the sediment transport problem from general physics. *USGS Special Paper*, 422.
- Barrière, J., Oth, A., Hostache, R., & Krein, A. (2015). Bed load transport monitoring using seismic observations in a low-gradient rural gravel bed stream. *Geophysical Research Letters*, *42*, 2294–2301. doi: 10.1002/2015GL063630
- Bottelin, P., Lèvy, C., Baillet, L., Jongmans, D., & Guèguen, P. (2013). Modal and thermal analysis of les arches unstable rock column (vercors massif, french alps). *Geophysical Journal International*, *194*, 849–858. doi: 10.1093/gji/ggt046
- Bunte, K., & Abt, S. (2005). Effect of sampling time on measured gravel bed load transport rates in a coarse-bedded stream. *Water Resources Research*, *41*, W11405. doi: 10.1029/2004WR003880
- Burtin, A., Bollinger, L., Vergne, J., Cattin, R., & Nabelek, J. L. (2008). Spectral analysis of seismic noise induced by rivers: A new tool to monitor spatiotemporal changes in stream hydrodynamics. *Journal of Geophysical Research*, *113*, B05301. doi: 10.1029/2007JB005034

- 506 Cohen, H., Laronne, J., & Reid, I. (2010). Simplicity and complexity of bed load
507 response during flash floods in a gravel bed ephemeral river: A 10 year field
508 study. *Water Resources Research*, *46*(11). doi: 10.1029/2010WR009160
- 509 Cook, K. L., Andermann, C., Gimbert, F., Adhikari, B. R., & Hovius, N. (2018).
510 Glacial lake outburst floods as drivers of fluvial erosion in the Himalaya. *Sci-
511 ence*, *362*(6410), 53–57. doi: 10.1126/science.aat4981
- 512 Cudden, J., & Hoey, T. B. (2003). The causes of bedload pulses in a gravel channel:
513 The implications of bedload grain size distributions. *Earth Surface Processes
514 and Landforms*, *28*, 1411–1428.
- 515 Dhont, B., & Ancey, C. (2018). Are bedload transport pulses in gravel bed rivers
516 created by bar migration or sediment waves? *Geophysical Research Letters*,
517 *45*, 5501–5508. doi: 10.1029/2018GL077792
- 518 Dietze, M. (2018). The R package 'eseis' – a software toolbox for environmental seis-
519 mology. *Earth Surface Dynamics*, *6*, 669–686. doi: 10.5194/esurf-6-669-2018
- 520 Dietze, M., Gimbert, F., Turowski, J., Stark, K., Cadol, D., & Laronne, J. (2019).
521 The seismic view on sediment laden ephemeral flows – modelling of ground
522 motion data for fluid and bedload dynamics in the Arroyo de los Piños [Com-
523 puter software manual]. Retrieved from [https://www.sedhyd.org/2019/
524 openconf/modules/request.php?module=oc_program&action=view.php&id=
525 99&file=1/99.pdf](https://www.sedhyd.org/2019/openconf/modules/request.php?module=oc_program&action=view.php&id=99&file=1/99.pdf) (Paper to SEDHYD conference)
- 526 Dietze, M., Turowski, J. M., Cook, K. L., & Hovius, N. (2017). Spatiotemporal pat-
527 terns, triggers and anatomies of seismically detected rockfalls. *Earth Surface
528 Dynamics*, *5*(4), 757–779. Retrieved from [https://www.earth-surf-dynam
529 .net/5/757/2017/](https://www.earth-surf-dynam.net/5/757/2017/) doi: 10.5194/esurf-5-757-2017
- 530 Einstein, H. (1950). The bedload function for sediment transportation in open chan-
531 nel flows. In *Technical report no. 1026*. United States Department of Agricul-
532 ture.
- 533 Geay, T., Belleudy, P., Habersack, C., Gervaise, H., Aigner, J., Kreisler, A., ...
534 Laronne, J. (2017). Passive acoustic monitoring of bedload flux in a large
535 gravel bed river. *Journal of Geophysical Research*, *128*, 528–545. doi:
536 10.1002/2016JF004112
- 537 Geay, T., Michel, L., Zanker, S., & Rigby, J. R. (2019). Acoustic wave propagation
538 in rivers: an experimental study. *Earth Surface Dynamics*, *7*(2), 537–548. doi:
539 10.5194/esurf-7-537-2019
- 540 Ghilardi, T., Franca, M., & Schleiss, A. J. (2014). Period and amplitude of bedload
541 pulses in a macrorough channel. *Geomorphology*, *221*, 95–103.
- 542 Gimbert, F., B.M., F., M.P., L., Tsai, V., & Johnson, J. (2019). Particle trans-
543 port mechanics and induced seismic noise in steep flume experiments with
544 accelerometer-embedded tracers. *Earth Surface Processes and Landforms*, *44*,
545 219–241. doi: 10.1002/esp.4495
- 546 Gimbert, F., Tsai, V. C., & Lamb, M. P. (2014). A physical model for seismic noise
547 generation by turbulent flow in rivers. *Journal of Geophysical Research*, *119*,
548 2209–2238. doi: 10.1002/2014JF003201
- 549 Gomez, B., Naff, R., & Hubbell, D. (1989). Temporal variations in bedload trans-
550 port rates associated with the migration of bedforms. *Earth Surface Processes
551 and Landforms*, *14*(4), 135–156.
- 552 Habersack, H., Kreisler, A., Rindler, R., Aigner, J., Seitz, H., Liedermann, M., &
553 Laronne, J. (2016). Integrative automatic and continuous bedload monitoring.
554 *Geomorphology*, *291*, 80–93. doi: 10.1016/j.geomorph.2016.10.020
- 555 Halfi, E., Deshpande, V., Johnson, J., Katoshevski, D., Reid, I., Storz-Peretz, Y., &
556 Laronne, J. (2018). Characterization of bed load discharge in flood bores and
557 very unsteady flows in an ephemeral channel. *E3S Web of Conferences*, *40*,
558 02036. doi: 10.1051/e3sconf/20184002036
- 559 Hildale, R., Carpenter, W., Goodwiller, B., Chambers, J., & Randle, T. (2014).
560 Installation of impact plates to continuously measure bed load: Elwha

- 561 river, washington, usa. *Journal of Hydraulic Engineering*, 141. doi:
562 10.1061/(ASCE)HY.1943-7900.0000975
- 563 Iseya, F., & Ikeda, H. (n.d.). Pulsations in bedload transport rates induced by a lon-
564 gitudinal sediment sorting: A flume study using sand and gravel mixtures. *Ge-*
565 *ografiska Annaler. Series A, Physical Geography*, 69.
- 566 James, S. R., Knox, H. A., Abbott, R. E., Panning, M. P., & Screaton, E. J. (ac-
567 cepted). Insights into permafrost and seasonal active-layer dynamics from
568 ambient seismic noise monitoring. *Journal of Geophysical Research: Earth*
569 *Surface*.
- 570 King, J. G., Emmett, W. W., Whiting, P. J., & Kenworthy, R. P. B. J. J. (2004).
571 Sediment transport data and related information for selected coarse-bed
572 streams and rivers in idaho. general technical report rmrs-gtr-131. In *Gen-*
573 *eral technical report rmrs-gtr-131* (p. 26). U.S. Department of Agriculture,
574 Forest Service, Rocky Mountain Research Station.
- 575 Laronne, J., Reid, I., Yitshak, Y., & Frostick, L. (1992). Recording bedload dis-
576 charge in a semiarid channel, nahal yatir, israel. *International Association of*
577 *Hydrological Sciences*, 210, 79–86.
- 578 Lisle, T., Cui, Y., Parker, G., Pizzuto, J., & Dodd, A. (2001). The dominance of
579 dispersion in the evolution of bed material waves in gravel-bedded rivers. *Earth*
580 *Surface Processes and Landforms*, 26, 1409–1420. doi: 10.1002/esp.300
- 581 Mizuyama, T., Laronne, J., Nonaka, M., Sawada, T., Satofuka, Y., Matsuoka, M.,
582 ... Tsuruta, K. (2010). Calibration of a passive acoustic bedload monitoring
583 system in japanese mountain rivers. *US Geological Survey Scientific Investiga-*
584 *tions Report*, 5091, 296-318.
- 585 Parker, G. (1990). Surface-based bedload transport relation for gravel rivers. *Journal*
586 *of Hydraulic Research*, 28, 417–436. doi: 10.1080/00221689009499058
- 587 RCoreTeam. (2015). R: A Language and Environment for Statistical Computing
588 [Computer software manual]. Vienna, Austria. Retrieved from [http://CRAN.R-](http://CRAN.R-project.org)
589 [project.org](http://CRAN.R-project.org)
- 590 Rickenmann, D. (2017). Bedload transport measurements with geophones, hy-
591 drophones and underwater microphones (passive acoustic methods). In
592 D. Tsutsumi & J. Laronne (Eds.), *Gravel bed rivers and disasters* (first edi-
593 tion ed., pp. 185–208). John Wiley & Sons.
- 594 Roth, D. L., Brodsky, E. E., Finnegan, N. J., Rickenmann, D., Turowski, J., &
595 Badoux, A. (2016). Bed load sediment transport inferred from seismic sig-
596 nals near a river. *Journal of Geophysical Research Earth Surface*, 121. doi:
597 10.1002/2015JF003782
- 598 Roth, D. L., Finnegan, N. J., Brodsky, E. E., Rickenmann, D., Turowski, J. M.,
599 Badoux, A., & Gimbert, F. (2017). Bed load transport and boundary rough-
600 ness changes as competing causes of hysteresis in the relationship between river
601 discharge and seismic amplitude recorded near a steep mountain stream. *Jour-*
602 *nal of Geophysical Research Earth Surface*, 122. doi: 10.1002/2016JF004062
- 603 Schmandt, B., Gaeuman, D., Stewart, R., Hansen, S., Tsai, V., & Smith, J. (2017).
604 Seismic array constraints on reach-scale bedload transport. *Geology*, 45, 299–
605 302. doi: 10.1130/G38639.1
- 606 Schumm, S. (1991). *To interpret the earth: Ten ways to be wrong*. Cambridge Uni-
607 versity Press.
- 608 Schumm, S. (2005). *River variability and complexity*. Cambridge University Press.
- 609 Tsai, V., Minchew, B., Lamb, M. P., & Ampuero, J.-P. (2012). A physical model
610 for seismic noise generation from sediment transport in rivers. *Geophysical Re-*
611 *search Letters*, 39, L02404. doi: 10.1029/2011GL050255
- 612 Tuszynski, J. (2014). catools: Tools: moving window statistics, gif, base64, roc auc,
613 etc. [Computer software manual]. Retrieved from [https://CRAN.R-project](https://CRAN.R-project.org/package=caTools)
614 [.org/package=caTools](https://CRAN.R-project.org/package=caTools) (R package version 1.17.1)
- 615 Welch, P. D. (1967). The use of fast fourier transform for the estimation of power

616

spectra: A method based on time averaging over short, modified periodograms.

617

IEEE Transactions on Audio and Electroacoustics, 15, 70–73.